Structural Chemistry (2021) 32:787–798
https://doi.org/10.1007/s11224-020-01650-5

ORIGINAL RESEARCH

A DFT quest for effects of fused rings on the stability of remote *N*-heterocyclic carbenes

Parvaneh Delir Kheirollahi Nezhad[1] · Leila Youseftabar-Miri[2] · Sheida Ahmadi[1] · Saeideh Ebrahimiasl[3,4] · Esmail Vessally[1]

Received: 2 June 2020 / Accepted: 22 September 2020 / Published online: 13 October 2020

Abstract

Assuming aromaticity (cyclic continuous conjugation, planarity, and obeying the Hückel 4n + 2 rule), effects of one and two fused six-membered heterocyclic rings are investigated on the energy lowering (stabilization) of 22 novel singlet (s) and triplet (t) carbenes, at B3LYP/AUG-cc-pVTZ and M06-2X/AUG-cc-pVTZ. Results display that (1) exclusive of triplet pyridine-4-ylidene, and s and t states, other species appear as ground state, so every s Hammick carbene exhibits more stability than its corresponding t state; (2) the highest stability is demonstrated by unsubstituted pyridine-4-ylidene as reference carbene, and the lowest stability is shown by carbene situated between two nitrogen heteroatoms of two fused rings, in a "W" arrangement; (3) regarding the relationship between carbenic center (CC) and substituted heteroatom, the order of stabilization for fused rings is *meta* > *para* > *ortho*; (4) regardless of how organized, fusion of one six-membered ring, in a given arrangement, has more stabilizing effect than two six-membered rings; (5) contrary to our expectation, t Hammick carbenes show higher band gap ($\Delta E_{\text{HOMO-LUMO}}$) than their corresponding s species; (6) based on the NICS (nuclear independent chemical shift) results, the least stable carbene has the most aromaticity in its pyridine ring; and (7) according to proposed homomolecular isodesmotic reactions, all s states are stabilized via π-donor/σ-acceptor substitution more than the t states.

Keywords Hammick carbene · Stability · Nucleophilicity · Aromaticity

Introduction

Carbenes as reactivate intermediates are of great current interest, because of their individual structural properties, their catalytic reactions in transition metal complexes or metal-free organocatalysts, their metallopharmaceuticals, and their coordination to p-block elements in many fields of applied chemistry [1, 2]. The size and substitution pattern can have a large effect on the properties of *N*-heterocyclic carbenes (NHCs) [3]. Initially, Buchner and Curtius discovered carbenes that seemed impossible to isolate [4]. Nevertheless, Bertrand successfully synthesized and isolated five-membered NHCs containing α-nitrogen atoms [4–8]. Kühn et al. synthesized and compared tetrazolylidenes with transition metal complexes [7]. Variation among normal and abnormal substitution pattern brings an effect on σ-donor abilities of the ligands (Scheme 1).

Substituent effects on the five-membered ring is investigated with imidazole-2-ylidene; imidazoline-2-ylidene; 1,2,4-triazole-5-ylidene; and tetrazole-5-ylidene [8]. Clearly, the number and position of substituted atoms are significant. The nucleophilicity (*N*), and global electrophilicity (ω) of the corresponding CC is decreased, and is increased, respectively, owing to the less inductive electron withdrawal from the neighboring carbon atom, and lack of p-donation, respectively [9–11]. Also, Kassaee et al. theoretically have compared steric

Electronic supplementary material The online version of this article (https://doi.org/10.1007/s11224-020-01650-5) contains supplementary material, which is available to authorized users.

✉ Sheida Ahmadi
sh.ahmadi_ch@yahoo.com

[1] Department of Chemistry, Payame Noor University, Tehran, Iran

[2] Department of Organic Chemistry, Faculty of Pharmaceutical Chemistry, Tehran Medical Sciences, Islamic Azad University, Tehran, Iran

[3] Department of Chemistry, Ahar Branch, Islamic Azad University, Ahar, Iran

[4] Industrial Nanotechnology Research Center, Tabriz Branch, Islamic Azad University, Tabriz, Iran

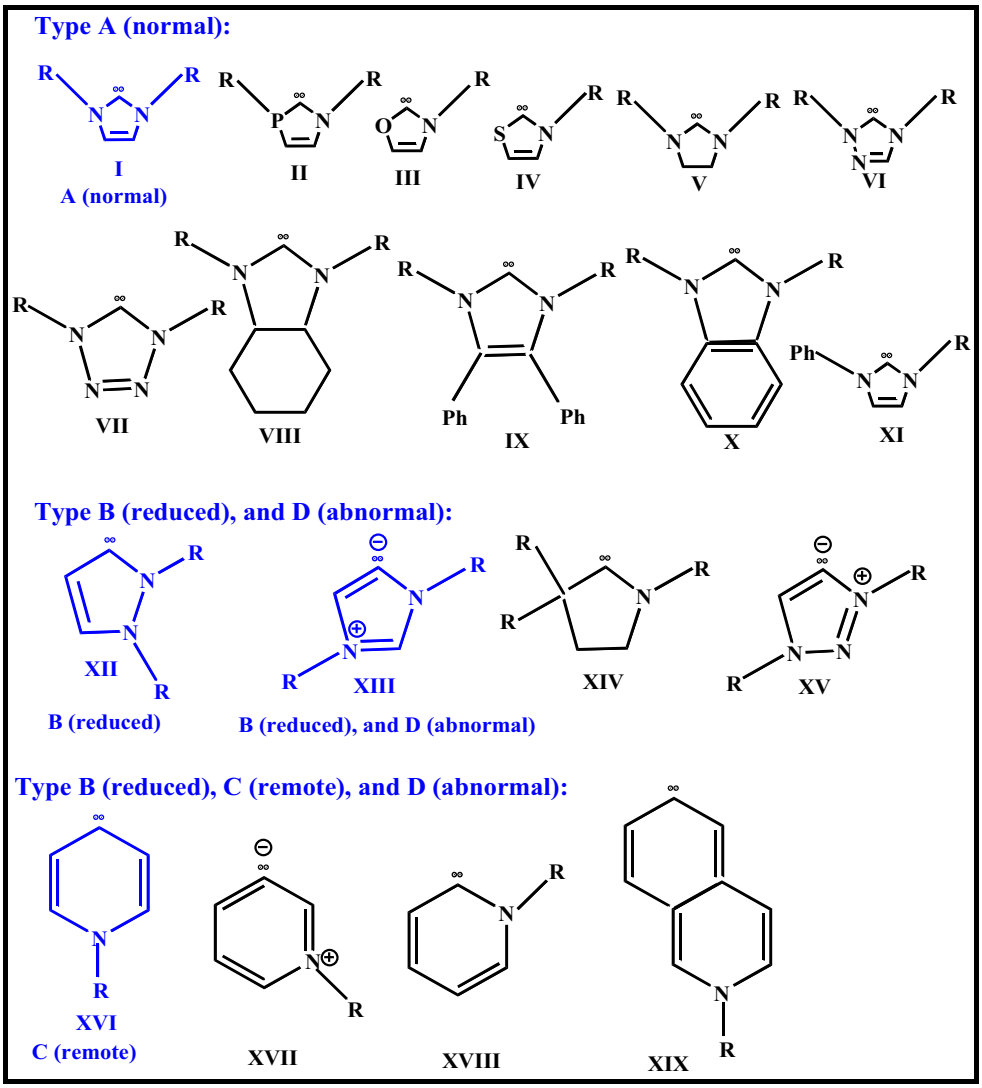

Scheme 1 Classes of NHCs including normal A, reduced nitrogen atom stabilized B (CAAC), remote C, and abnormal D

effects of tetrazol-5-ylidens and diaminocarbenes [12, 13]. They have reported *N* is a crucial factor for the coordination of NHCs' excellent σ-donors to transition metal complexes, *N* increases as the size of the substituent increases, *ω* trend takes on an exactly opposite direction, and both normal and abnormal carbenes become more stable in the presence of heteroatoms. Evidently, the nitrogen-substituents or other groups situated adjacent to CC have the largest influence on the steric environment at the CC. In this manuscript, we try to respond to the important question of: "How fused rings effect on the stability of Hammick carbene?" Hence, we are probed normal substituted pyridine-4-ylidenes (**1**–**5**) and abnormal derivatives (**6**–**11**) (Scheme 2).

That is, three classes of pyridine-derived NHCs are identified: normal, abnormal, and normal remote (rNHCs). The difference among these three classes is the relationship between substituted heteroatom and CC, which is *ortho*, *meta*, and *para*, respectively [9–18].

Computational methods

The reliability of various, the most popular density functional theory (DFT) [19–22], B3LYP [23–30], and M06-2X [31] is already evaluated for the study of bond dissociation energies, heats of formation, molecular properties, geometrical parameters, polarizability, and hyperpolarizability not only for atoms and small molecules but also for large systems [36–42]. Conversely, the advantages of using DFT for determining single-bond torsional potentials in π-conjugated systems are less obvious. In accordance with the previous calculations, the B3LYP [23–27] method has been well-used to the theoretical valuations on divalent species so that it could provide rather responsible results contrasted to those achieved through various basis sets [41–46]. In this work, full geometry optimization of Hammick s and t carbenes is carried out without any symmetry constraints using the GAMESS program package [47, 48]. The restricted hybrid functional B3LYP and M06-2X methods are employed for s states, and

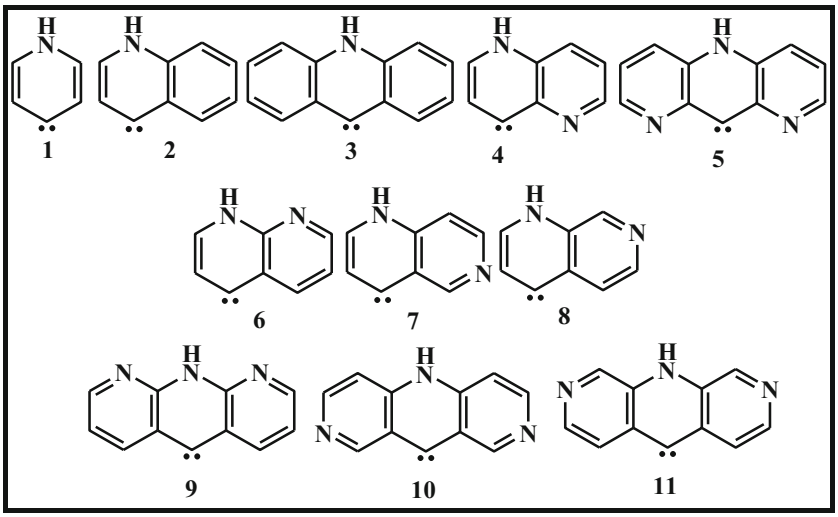

Scheme 2 Hammick carbenes containing pyridine-4-ylidenes (1–5) and abnormal derivatives (6–11)

unrestricted broken spin-symmetry UB3LYP and UM06-2X are used for t states due to its excellent performance-to-cost ratio as compared with correlated wave function theory [19–27]. The applied 6-311+G* basis set is confined of Pople's famous basis set and an extra plus owing to the significance of diffuse functions [49–52]. To reach more accurate energetic data, single-point calculations are accomplished at (U)B3LYP/AUG-cc-pVTZ//(U)B3LYP/6-311+G*. In order to confirm the nature of the stationary species, the harmonic vibration frequency (υ_{min}) calculations are carried out, at (U)M06-2X/AUG-cc-pVTZ//(U)M06-2X/6-311+G* [53, 54]. The natural bond orbital (NBO) calculations involving the charge distributions are done at the (U)M06-2X/AUG-cc-pVTZ [55–58]. To obtain the magnetic data, NICS calculations are applied at GIAO/B3LYP/AUG-cc-pVTZ [59–61] including NICS (0, 0.5, 1, 1.5, 2) values, at rings centers, 0.5, 1.0, 1.5, and 2.0 Å above the plane of rings showing NICS1 for singlet pyridine-4-ylidene ring, **1**, along with NICS2 (values in italic) for its fused rings, respectively. The nucleophilicity index, N, is calculated as $N = \Delta E_{HOMO(Nu)} - \Delta E_{HOMO(TCNE)}$, where tetracyanoethylene (TCNE) is preferred as the reference [62]. The global electrophilicity (ω), chemical potential (μ), and chemical hardness (η) are obtained via the expression of $\omega = (\mu^2/2\eta)$, $\mu = (E_{HOMO} + E_{LUMO})/2$, and $\eta = E_{HOMO} - E_{LUMO}$ [63–65]. DFT calculations are implemented to identify the stability of the scrutinized carbenes through appropriate isodesmic reactions.

Results and discussion

Succeeding our search for stable NHCs, we have probed s and t states of pyridine-4-ylidene, and its derivatives, (**1**–**11**, Scheme 2) and contrasted their stability based on singlet-

Table 1 The minimum vibrational frequency (υ_{min} in cm^{-1}), total energy (E in *a.u.*) calculated for s and t carbenes at M06-2X/AUG-cc-pVTZ, their energy separation ($\Delta E_{s-t} = E_t - E_s$ in kcal/mol) at B3LYP/AUG-cc-pVTZ (values in upright), and M06-2X/AUG-cc-pVTZ (values in italic), and their stabilizing energy (ΔE in kcal/mol) compared with the parent pyridine-4-ylidene, **1**, at B3LYP/AUG-cc-pVTZ

	υ_{min}	E	ΔE_{s-t}	ΔE		υ_{min}	E	ΔE_{s-t}	ΔE
1s	317.1	− 248.25632	22.5, *22.0*	0.00, 0.00	**7s**	155.0	− 417.98158	14.0, *14.5*	− 8.5, − *7.5*
1t	− 222.1	− 248.22118			**7t**	146.8	− 417.95852		
2s	156.2	− 401.94159	14.9, *15.6*	− 7.6, − *6.4*	**8s**	156.5	− 417.97848	12.5, *12.8*	− 10.0, − *9.2*
2t	136.7	− 401.91679			**8t**	139.5	− 417.95804		
3s	82.1	− 555.62634	10.5, *11.9*	− 12.0, − *10.1*	**9s**	86.9	− 587.72618	8.6, *10.0*	− 13.9, − *12.0*
3t	74.7	− 555.60742			**9t**	82.2	− 587.71017		
4s	132.3	− 417.97278	9.1, *9.5*	− 13.4, − *12.5*	**10s**	81.2	− 587.70792	12.0, *11.4*	− 10.5, − *10.6*
4t	140.0	− 417.95762			**10t**	75.8	− 587.68969		
5s	80.7	− 587.68772	0.3, *1.1*	− 22.2, − *20.9*	**11s**	79.4	− 587.69734	6.9, *6.4*	− 15.6, − *15.6*
5t	80.2	− 587.68596			**11t**	75.5	− 587.68710		
6s	163.5	− 417.99228	13.8, *14.0*	− 8.7, − *8.0*					
6t	153.8	− 417.97000							

Table 2 The frontier molecular orbital energies (E_{HOMO}, E_{LUMO} in *a.u.*) and their corresponding band gaps ($\Delta E_{HOMO-LUMO}$ in kcal/mol) calculated for s and t carbenes at B3LYP/AUG-cc-pVTZ (values in upright), and M06-2X/AUG-cc-pVTZ (values in italic)

Species	E_{HOMO}	E_{LUMO}	$\Delta E_{HOMO-LUMO}$	Species	E_{HOMO}	E_{LUMO}	$\Delta E_{HOMO-LUMO}$
1s	− 0.1685	− 0.0559	70.7, *70.4*	**7s**	− 0.1857	− 0.0865	62.3, *63.4*
1t	− 0.2617	− 0.0779	115.4, *113.9*	**7t**	− 0.2470	− 0.0968	94.3, *93.2*
2s	− 0.1732	− 0.0742	62.1, *63.4*	**8s**	− 0.1860	− 0.0917	59.2, *55.8*
2t	− 0.2289	− 0.0858	89.8, *90.5*	**8t**	− 0.2415	− 0.0984	89.8, *88.5*
3s	− 0.1803	− 0.0870	58.6, *59.6*	**9s**	− 0.1943	− 0.1054	55.8, *54.2*
3t	− 0.2173	− 0.0925	78.3, *77.5*	**9t**	− 0.2477	− 0.1090	87.0, *85.9*
4s	− 0.1742	− 0.0879	54.2, *54.8*	**10s**	− 0.2021	− 0.1070	60.1, *59.6*
4t	− 0.2522	− 0.0895	102.1, *104.1*	**10t**	− 0.2520	− 0.1124	87.6, *88.2*
5s	− 0.1811	− 0.1076	46.1, *46.9*	**11s**	− 0.2042	− 0.1191	53.6, *54.8*
5t	− 0.2456	− 0.1003	91.2, *92.5*	**11t**	− 0.2381	− 0.1155	77.0, *79.4*
6s	− 0.1813	− 0.0868	59.3, *60.3*				
6t	− 0.2532	− 0.0956	98.9, *97.7*				

triplet energy difference (ΔE_{s-t}), structural parameters such as bond length (R), divalent angle (A), dihedral angle (D), dipole moment (DM), NBO charge distribution, and MEP maps at B3LYP/AUG-cc-pVTZ, and M06-2X/AUG-cc-pVDZ which approve the higher stability of singlet carbenes. Beneficial results are attained from these species including υ_{min}, N, ω, μ, and $\Delta E_{HOMO-LUMO}$. Additionally, we have estimated relative stability through aromaticity (NICS), and isodesmic reactions. Except for **1t** with an imaginary frequency of − 222.1 cm^{-1}, all full-optimized geometries turn out as minima on their potential energy surfaces for displaying no negative force constant (Table 1).

Fortunately, both s and t states of **2**, **4**, **6**, **7**, and **8** carbenes have υ_{min} values more than 100 cm^{-1} [66]. All s Hammick carbenes appear as ground state, showing more stability than their corresponding t congeners. In this work, because of the reliability between the thermodynamic characters (ΔE_{s-t}, ΔH_{s-t}, and ΔG_{s-t}) also for the sake of time saving, we confine our results and discussion to ΔE_{s-t}. The total stability trend recommended by these parameters is **1** (22.5) > **2** (14.9) > **7** (14.0) ≥ **6** (13.8) > **8** (12.5) > **10** (12.0) > **3** (10.5) > **4** (9.1) > **9** (8.6) > **11** (6.9) > **5** (0.3 kcal/mol). There is an inconsistent relationship among $\Delta E_{HOMO-LUMO}$ trend of s species; **1s** (70.7) > **7s** (62.3) ≥ **2s** (62.1) > 10s (60.1) > **6s** (59.3) ≥ **8s** (59.2) > **3s** (58.6) > **9s** (55.8) > **4s** (54.2) > **11s** (53.6) > **5s** (46.1 kcal/mol) and $\Delta E_{HOMO-LUMO}$ trend of t species; **1t** (115.4) > **4t** (102.1) > **6t** (98.9) > **7t** (94.3) > **5t** (91.2) > **2t** (89.8) = **8t** (89.8) > **10t** (87.6) > **9t** (87.0) > **3t** (78.3) > **11t** (77.0 kcal/mol) (Table 2).

Completely planar geometries are demonstrated by all species, while their symmetries are C_s and/or C_1 (Table 3).

Located non-bonding electrons in the σ-orbital of CC, which is orthogonal to π-system and the ring current, leads to higher DM in s structures (**1s**–**11s**) than their corresponding triplets (about 1.5–3 times). For example, **5s** (9.56 Debye) displays a higher DM than **5t** (6.53 Debye). Also, in polar environment, **9s** (1.93 Debye) and **9t** (0.97 Debye) are expected to be stabilized to a smaller extent than the other species. The average polarizability (α), as a criteria of interaction of one molecule with its surrounding polar species, increases from 64.31 *a.u.* for **1t** to 179.66 *a.u.* for **3t** compared with **1s**, and **3s** (68.34, and 174.23 *a.u.*, respectively). This result reveals that substituting the mentioned groups leads to increasing α and activity of fused carbenes (Table 3). Triplet carbenes have less N than their corresponding s states, showing the most and the least value for **1s** (4.87 eV) and **1t** (2.34 eV), respectively (Table 4).

More participation of the unpaired non-bonding electron on CC in delocalization causes the s structures more prone to N than their related t states. Here, the substituent effect plays a different role in ω of the scrutinized s and t Hammick

Table 3 The calculated dipole moment (DM in Debye), polarizability (α in *a.u.*) and point group (PG) of s and t carbenes at M06-2X/AUG-cc-pVTZ

Species	DM	(α)	PG		D.M.	(α)	PG
1s	6.96	68.34	C_s	**7s**	7.43	109.76	C_s
1t	2.73	64.31	C_s	**7t**	4.86	110.37	C_s
2s	6.21	116.77	C_s	**8s**	5.50	110.16	C_s
2t	2.62	117.42	C_s	**8t**	3.68	110.64	C_s
3s	5.18	174.23	C_1	**9s**	1.93	172.45	C_1
3t	2.12	179.66	C_1	**9t**	0.97	161.35	C_1
4s	8.38	111.41	C_s	**10s**	7.16	158.44	C_1
4t	4.94	113.24	C_s	**10t**	4.29	163.21	C_1
5s	9.56	162.44	C_1	**11s**	2.96	159.55	C_1
5t	6.53	170.59	C_1	**11t**	1.24	163.75	C_1
6s	4.06	110.75	C_1				
6t	1.38	114.08	C_1				

Table 4 The calculated nucleophilicity index (N), global electrophilicity (ω), chemical potential (μ), and global hardness (η) in eV, for s carbenes, at B3LYP/AUG-cc-pVTZ

Species	N	ω	μ	η
1s	4.87	1.52	− 3.05	3.07
1t	2.34	2.13	− 4.62	5.00
2s	4.75	2.10	− 3.37	2.69
2t	3.23	2.35	− 4.28	3.89
3s	4.55	2.60	− 3.64	2.54
3t	3.55	2.62	− 4.21	3.391
4s	4.72	2.70	− 3.57	2.35
4t	2.60	2.44	− 4.65	4.43
5s	4.53	3.86	− 3.93	2.00
5t	2.78	2.80	− 4.71	3.95
6s	4.53	2.59	− 3.65	2.57
6t	2.57	2.63	− 4.75	4.29
7s	4.41	2.54	− 3.70	2.70
7t	2.74	3.70	− 4.68	4.09
8s	4.40	2.78	− 3.78	2.57
8t	2.89	2.75	− 4.62	3.89
9s	4.17	3.43	− 4.08	2.42
9t	2.72	3.12	− 4.85	3.77
10s	3.95	3.39	− 4.20	2.61
10t	2.60	3.24	− 4.96	3.80
11s	3.90	4.16	− 4.40	2.32
11t	2.98	3.47	− 4.81	3.34

carbenes. The N data show no noticeable correlations with the corresponding ω values for s and t species. For instance, **11s** shows higher ω (4.16 eV) than **11t** (3.47 eV), while **1s** shows lower ω (1.52 eV) than **1t** (2.13 eV). Also, every s carbene shows lower absolute value of chemical potential ($|\mu|$), and global hardness (η) as global reactivity descriptor than its corresponding t structure. Succeeding our attention to stable synthesized carbenes, here, we compare the substituent effect on the N and ω of some of common NHCs with five-membered rings (**12s**–**19s**, Scheme 3).

Because of the smaller carbenic angle, all five-membered rings exhibited less N and less ω than the six-membered rings (Table 5).

The highest N and the highest ω of the synthesized NHCs are considered for **12s** and **17s** with the values of 3.78 and 1.56 eV, respectively. We hope the higher N of six-membered carbenes along with their thermodynamic stability will make them worthy of synthetic attentions. The overall aromaticity, according to NICS1 values for pyridine-4-ylidene rings and NICS2 values for fused rings, is considered for substituted species specially **2s** and **5s** more than those of unsubstituted species, **1** (Table 6).

The trend of aromaticity for the parent unsubstituted molecules is **1** < **2** < **3**, and for their corresponding substituted species is *ortho* > *meta* > *para*. However, substitution increases differences in aromaticity between the parent molecules (**1**, **2**, and **3**) and their corresponding derivatives. In addition, by going down from **1s** to **3s** and from **1t** to **3t**, the electron density distribution on CC decreases (− 0.727, − 0.681, − 0.156, − 0.276, − 0.074, and 0.456 e, respectively, Figs. 1 and 2 and S1–S2).

Contrary to benzene molecule, the pyridine group increases the electron density distribution on CC, revealing the most

Scheme 3 The common NHCs 12–19

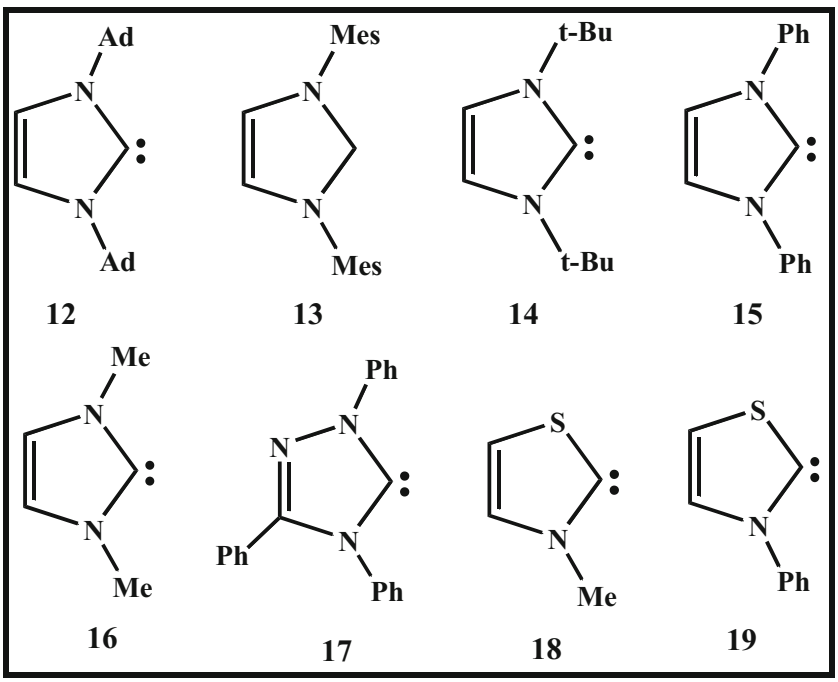

Table 5 The E_{HOMO} and E_{LUMO} energies in *a.u.*, *N*, and ω in eV for the s synthesized NHCs, at B3LYP/AUG-cc-pVTZ (see Scheme 3)

Species	E_{HOMO}	E_{LUMO}	*N*	ω
12s	− 0.20751	− 0.01858	3.78	0.92
13s	− 0.21753	− 0.01858	3.50	0.95
14s	− 0.20902	− 0.01098	3.74	0.83
15s	− 0.22738	− 0.03619	3.23	1.24
16s	− 0.21693	− 0.00817	3.52	0.82
17s	− 0.23036	− 0.05407	3.15	1.56
18s	− 0.23188	− 0.02357	3.11	1.06
19s	− 0.23474	− 0.04272	3.03	1.36

negative charge (−2.774 and − 1.526 e) for **5s**, and **5t**, respectively. Hence, pyridine ring has the weaker resonance stabilization than benzene (resonance energy in pyridine and benzene is 28.0 and 35.8 kcal/mol, respectively) [67]. Indeed, N_{LP} in the plane of the ring as the π-electron donoring group especially in a "W" arrangement has a more effect on charge distribution of s species than those of t species by more strongly interacting with the ring π-system.

Here, the electrostatic potential values of MEP maps are specified with different intensities for s carbenes compared with their corresponding t states in the range of − 0.0318 *a.u.* (deepest red) to + 0.0318 *a.u.* (deepest blue) (Figs. 3 and 4, and S3–S4) [37–40, 68, 69].

Also, MEP plots of both s and t states indicate blue color for hydrogen atoms via their positive charges, red color for carbon atoms via their negative charges, and the electron cloud in middle of ring(s). Also, MEP maps of s and t states display symmetrically and differentially electron current in the centers of the rings. As abovementioned, conjugation of the nitrogen s lone pairs with the vacant p orbitals of the CC in the most delocalized species, i.e., **5s** and **5t** increase their stability individually and decrease the corresponding ΔE_{s-t}. The electron-donating N_{LP} in the plane of the ring affects inversely charge distribution and electrostatic potential on the surfaces of **9s**, **10s**, **11s**, **9t**, **10t**, and **11t**, that is when nitrogen atoms of pyridine are placed far from reach in *meta* and *para* positions of CC via decreasing the effective π-overlap and the resulted aromaticity.

Based on suggested homomolecular isodesmotic reactions (Scheme 4) [70, 71], ΔE_s and ΔE_t are the energy released by s and t carbenes when the corresponding CC is converted to a saturated carbon via addition of two hydrogen atoms from the corresponding homomolecular saturated carbon; also, ΔE_{total} and $\Delta E_{relative}$ are defined as $\Delta E_t - \Delta E_s$ and $\Delta E_s/\Delta E_t$, respectively (Table 7).

We considered stabilization of both s and t carbenes, although with different degrees. The more heat of

Table 6 The NICS (0, 0.5, 1, 1.5, 2) values in ppm showing NICS1 (values in upright), for pyridine-4-ylidene ring, **1**, and NICS2 (values in italic) for its fused rings, respectively, at GIAO/B3LYP/AUG-cc-pVTZ

Structures	NICS1 (0) *NICS2 (0)*	NICS1 (0.5) *NICS2 (0.5)*	NICS1 (1) *NICS2 (1)*	NICS1 (1.5) *NICS2 (1.5)*	NICS1 (2) *NICS2 (2)*
1s	− 8.71	− 8.49	− 9.77	− 7.40	− 4.74
2s	− 6.44	− 9.07	− 10.08	− 7.62	− 5.02
	− 8.32	*− 10.17*	*− 10.42*	*− 7.72*	*− 5.02*
3s	− 7.17	− 9.42	− 10.07	− 7.58	− 5.12
	− 7.71	*− 9.54*	*− 9.92*	*− 7.48*	*− 4.95*
4s	− 7.43	− 9.98	− 10.82	− 8.17	− 5.41
	− 7.47	*− 9.76*	*− 10.37*	*− 7.79*	*− 5.14*
5s	− 10.30	− 12.27	− 12.27	− 9.11	− 6.12
	− 6.64	*− 8.98*	*− 9.77*	*− 7.41*	*− 4.95*
6s	− 6.92	− 9.38	− 10.30	− 7.87	− 5.27
	− 7.11	*− 9.42*	*− 10.15*	*− 7.68*	*− 5.09*
7s	− 6.94	− 9.35	− 10.36	− 7.84	− 5.23
	− 7.13	*− 9.40*	*− 10.12*	*− 7.69*	*− 5.19*
8s	− 6.82	− 9.44	− 10.22	− 7.76	− 5.42
	− 7.05	*− 9.44*	*− 10.11*	*− 7.66*	*− 5.19*
9s	− 7.96	− 9.95	− 10.45	− 8.04	− 5.57
	− 6.22	*− 8.43*	*− 9.51*	*− 7.28*	*− 4.89*
10s	− 7.99	− 9.90	− 10.55	− 8.24	− 5.50
	− 6.36	*− 8.63*	*− 9.74*	*− 7.32*	*− 4.95*
11s	− 7.76	− 9.98	− 10.35	− 8.41	− 5.54
	− 6.24	*− 8.66*	*− 9.62*	*− 7.46*	*− 4.98*

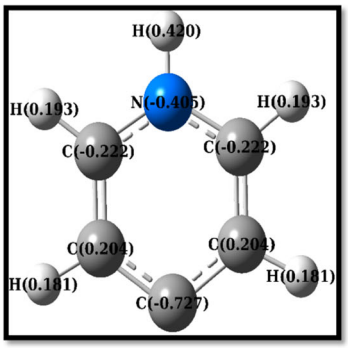

1s

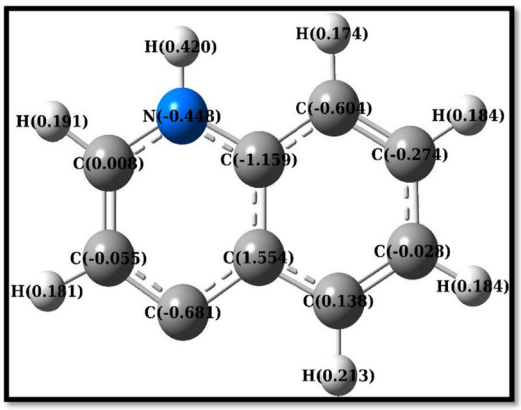

2s

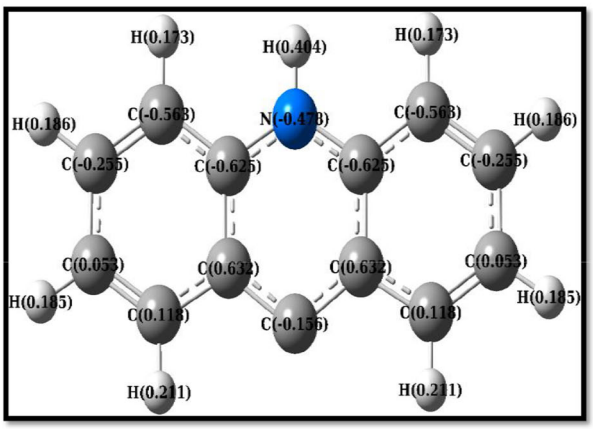

3s

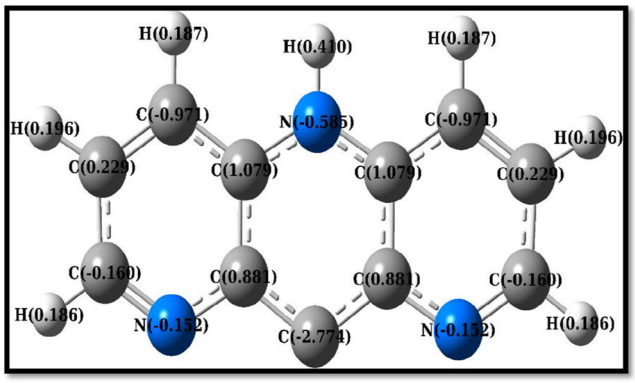

5s

Fig. 1 The NBO charge distribution on C, N, and H atoms of selected s species (**1s**, **2s**, **3s**, and **5s**) at M06-2X/AUG-cc-pVTZ

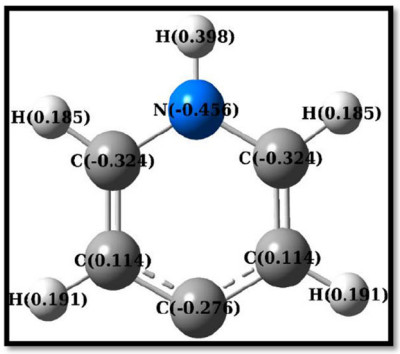

1t

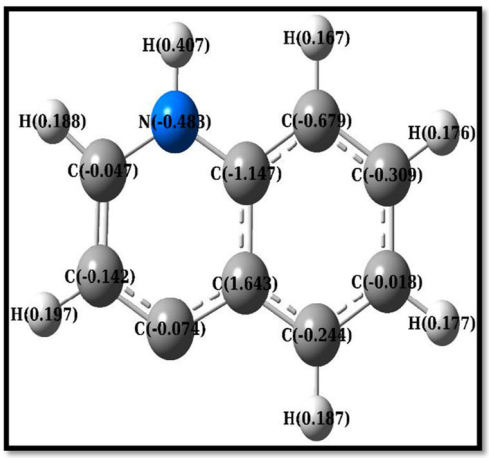

2t

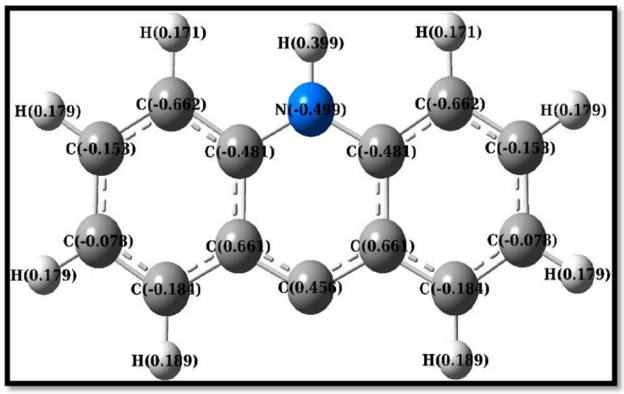

3t

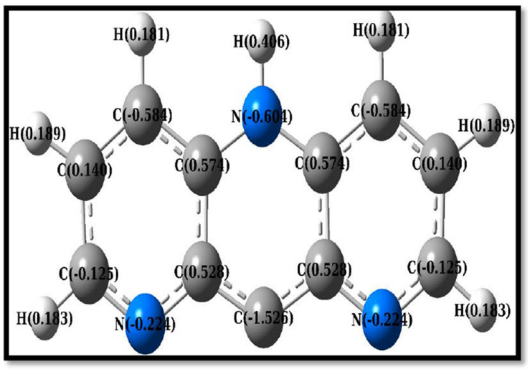

5t

Fig. 2 The NBO charge distribution on C, N, and H atoms of selected t species (**1t**, **2t**, **3t**, and **5t**) at M06-2X/AUG-cc-pVTZ

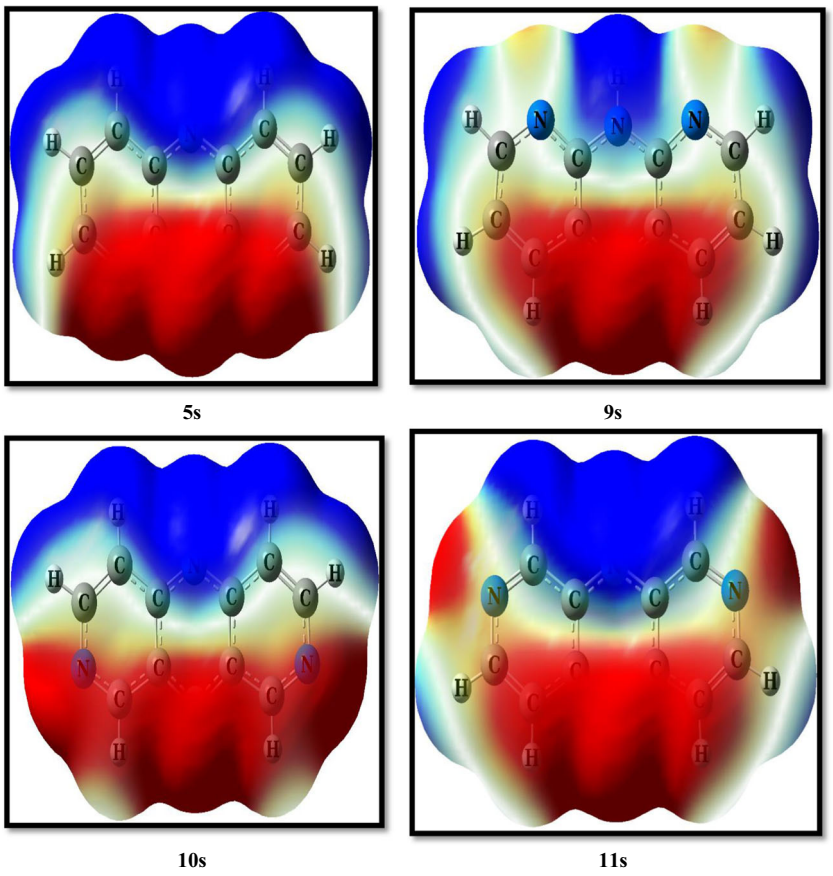

Fig. 3 The resulted MEP maps of selected s species (**5s**, **9s**, **10s**, and **11s**) at M06-2X/AUG-cc-pVTZ

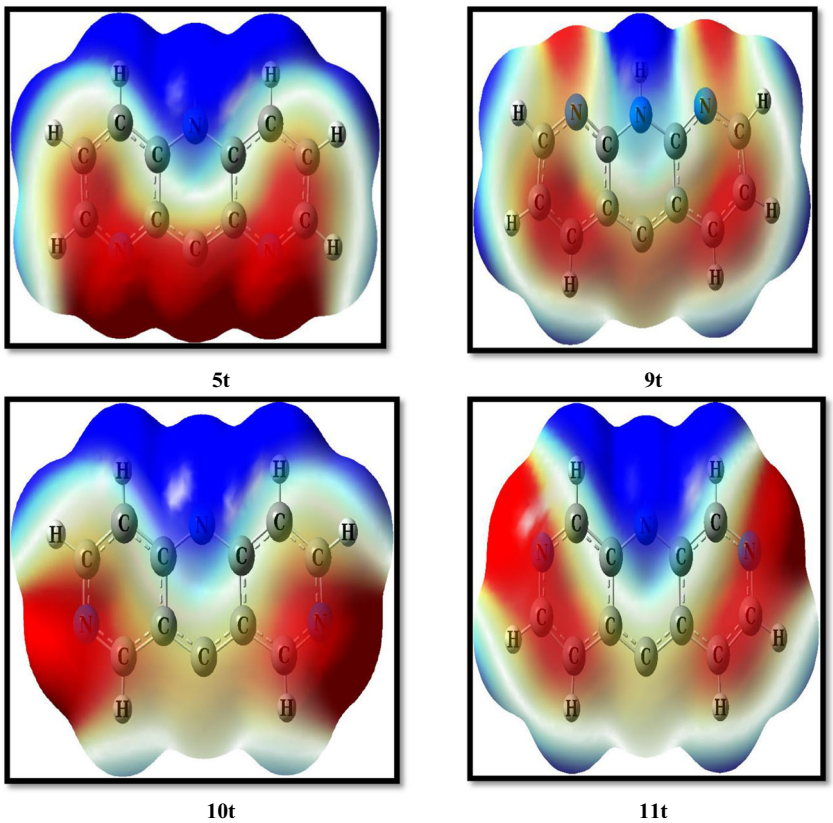

Fig. 4 The resulted MEP maps of selected t species (**5t**, **9t**, **10t**, and **11t**) at M06-2X/AUG-cc-pVTZ

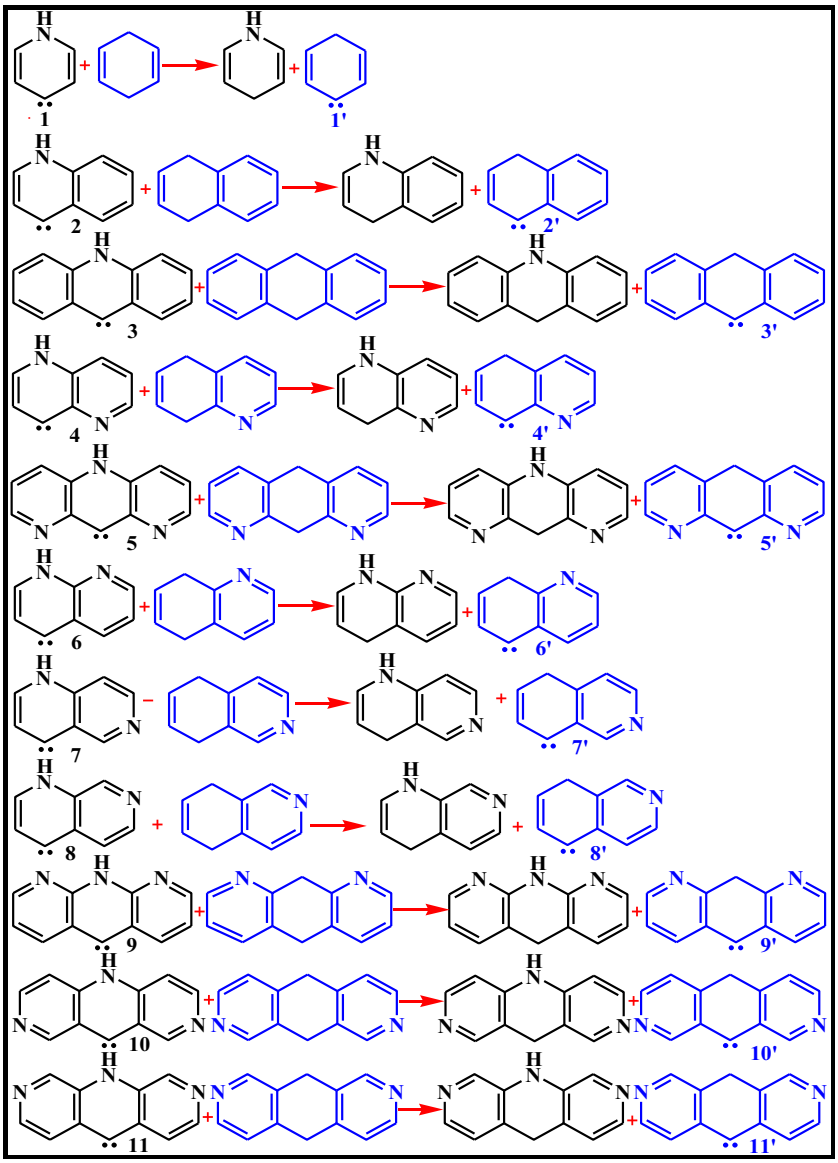

Scheme 4 The suggested isodesmic reactions for Hammick s and t carbenes **1**–**11**

Table 7 The substituent effect on the stability of s and t carbenes (ΔE_s, ΔE_t, respectively, $\Delta E_{total} = \Delta E_t - \Delta E_s$ and $\Delta E_{relative} = \Delta E_s/\Delta E_t$) in kcal/mol, at B3LYP/AUG-cc-pVTZ, based on the corresponding isodesmic reactions (see Scheme 4)

Carbenes	ΔE_s	ΔE_t	ΔE_{total}	$\Delta E_{relative}$
1	28.2	2.6	− 25.6	10.8
2	24.8	6.9	− 17.9	3.6
3	16.1	5.6	− 10.5	2.9
4	21.7	7.8	− 13.9	2.8
5	14.8	5.5	− 9.3	2.7
6	24.4	8.3	− 16.1	2.9
7	24.8	6.9	− 17.9	3.6
8	12.2	1.3	− 10.9	9.4
9	13.8	4.4	− 9.4	3.1
10	12.4	1.5	− 10.9	8.3
11	14.0	4.6	− 9.4	3.0

hydrogenation, the lower stability it has. The s species are stabilized more than the t states. The trends of absolute value of ΔE_{total} as well as $\Delta E_{relative}$ are somewhat consistent with the ΔE_{s-t} results; $|\Delta E_{total}|$: **1** (25.6) > **2** (17.9) = **7** (17.9) > **6** (16.1) > **4** (13.9) > **10** (10.9) = **8** (10.9) > **3** (10.5) > **9** (9.4) = **11** (9.4) ≥ **5** (9.3 kcal/mol). Evidently, compared with the completely conjugated carbenes **1**–**11**, the designed non-planar carbenes **1′**–**11′** only benefit from substitutient effects of fused benzene or pyridine rings with contribution of non-planar cyclohexa-2,5-dienic moiety. The absolute values of ΔE_{total} along with $\Delta E_{relative}$ seem much more (approximately 1.4–2.7 times) in unsubstituted carbene, **1**, than those of other substituted carbene, **2**–**11**, perhaps owing to the higher electronic energy barrier to planarity of N—atom in two rings compared with one ring.

Conclusion

Using B3LYP/AUG-cc-pVTZ and M06-2X/AUG-cc-pVTZ computations, 22 s and t Hammick carbenes (**1**–**11**) were inspected. Some of thermodynamic and kinetic factors including ΔE_{s-t}, ΔE, $\Delta E_{HOMO\text{-}LUMO}$, DM, α, N, ω, μ, η, NICS, NBO charge, MEP plots, and relative energies of isodesmic reactions (ΔE_s, ΔE_t, and ΔE_{total}) support differently substitution effect on s and t states. Apart from t pyridine-4-ylidene, all studied Hammick carbenes emerge as minima, and s states display more thermodynamic stability than the corresponding t states. The most stable carbene is unsubstituted s pyridine-4-ylidene, and the least stable species is considered with CC situated by two nitrogen heteroatoms of two fused rings, in a "W" arrangement. According to the situation of CC and heteroatoms, stabilization for fused rings is *meta* more than *para*, and *para* more than *ortho*; also, the substitution effect of one six-membered ring is significant than that of two six-membered rings. Every t state exhibits higher kinetic stability than its corresponding s state. Regarding to proposed isodesmic reactions, all s states are stabilized through π-donor/σ-acceptor substitution, more than the corresponding t states.

Compliance with ethical standards

Conflict of interest The authors declare that they have no conflicts of interest.

References

1. Danopoulos AA, Simler T, Braunstein P (2019) N-Heterocyclic carbene complexes of copper, nickel, and cobalt. Chem Rev 119(6):3730
2. Smith CA, Narouz MR, Lummis PA, Singh I, Nazemi A, Li C-H, Crudden CM (2019) N-Heterocyclic carbenes in materials chemistry. Chem Rev 119(88):4986
3. Melaimi M, Soleilhavoup M, Bertrand G (2010) Stable cyclic carbenes and related species beyond diaminocarbenes. Angew Chem Int Ed 49:8810
4. Buchner E, Curtius T (1885) Ueber die Einwirkung von Diazoessigäther auf aromatische Kohlenwasserstoffe. Ber Dtsch Chem Ges 8:2377
5. Igau A, Grützmacher H, Baceiredo A, Bertrand G (1988) Analogous .alpha.,.alpha.′-bis-carbenoid, triply bonded species: synthesis of a stable .lambda.3-phosphino carbene-.lambda.5-phosphaacetylene. J Am Chem Soc 110:6463
6. Bourissou D, Guerret O, Gabbaï FP, Bertrand G (2000) Stable Carbenes. Chem Rev 100:39
7. Schaper L-A, Wei X, Altmann PJ, Öfele K, Pöthig A, Drees M, Mink J, Herdtweck E, Bechlars B, Herrmann WA, Kühn FE (2013) Synthesis and comparison of transition metal complexes of abnormal and normal tetrazolylidenes: a neglected ligand species. Inorg Chem 52:7031
8. Schumacher M, Goldfuss B (2015) Quantifying N-heterocyclic carbenes as umpolung catalysts in the benzoin reaction: balance between nucleophilicity and electrophilicity. New J Chem 39:4508
9. Nelson DJ, Nolan SP (2013) Quantifying and understanding the electronic properties of N-heterocyclic carbenes. Chem Soc Rev 42:6723
10. Huynh HV, Frison G (2013) Electronic structural trends in divalent carbon compounds. J Org Chem 78:328
11. Frison G, Huynh HV, Bernhammer JC (2013) Electronic structure trends in N-heterocyclic carbenes (NHCs) with varying number of nitrogen atoms and NHC—transition-metal bond properties. Chem Eur J 19:12892
12. Rezaee N, Ahmadi A, Kassaee MZ (2016) Nucleophilicity of normal and abnormal N-heterocyclic carbenes at DFT: steric effects on tetrazole-5-ylidenes. RSC Adv 6:13224
13. Khorshidvand N, Kassaee MZ, Ahmadi AA, Cummings PT (2018) Steric effects on normal and abnormal acyclic, cyclic-saturated, and cyclic-unsaturated diaminocarbenes using DFT method. J Phys Org Chem 32:e3898
14. Schuster O, Yang L, Raubenheimer HG, Albrecht M (2009) Beyond conventional N-heterocyclic carbenes: abnormal, remote, and other classes of NHC ligands with reduced heteroatom stabilization. Chem Rev 109:3445
15. Han Y, Huynh HV (2007) Preparation and characterization of the first pyrazole-based remote N-heterocyclic carbene complexes of palladium(II). Chem Commun 10:1089
16. Schneider SK, Rentzsch CF, Krüger A, Raubenheimer HG, Herrmann WA (2007) Pyridin- and quinolinylidene nickel carbene complexes as effective catalysts for the Grignard cross-coupling reaction. J Mol Catal A Chem 265:50
17. Schneider SK, Roembke P, Julius GR, Loschen C, Raubenheimer HG, Frenking G, Herrmann WA (2005) Extending the NHC concept: C–C coupling catalysis by a PdII carbene (r NHC) complex with remote heteroatoms. Eur J Inorg Chem 15:2973
18. Schneider SK, Julius GR, Loschen C, Raubenheimer HG, Frenking G, Herrmann WA (2006) A first structural and theoretical comparison of pyridinylidene-type rNHC (remote N-heterocyclic carbene) and NHC complexes of Ni(II) obtained by oxidative substitution. Dalton Trans 9:1226
19. Chong DP (1997) Recent advances in density functional methods, parts I and II. World Scientific, Singapore.
20. Barone V, Bencini A (1999) Recent advances in density functional methods, part III. World Scientific, Singapore
21. Adamo C, Matteo A d, Barone V (2000) From classical density functionals to adiabatic connection methods. The state of the art. Adv Quantum Chem 36:45
22. Ess DH, Houk KN (2005) Activation Energies of pericyclic reactions: performance of DFT, MP2, and CBS-QB3 methods for the prediction of activation barriers and reaction energetics of 1,3-dipolar cycloadditions, and revised activation enthalpies for a standard set of hydrocarbon pericyclic reactions. J Phys Chem A 109:9542
23. Becke AD (1988) Density-functional exchange-energy approximation with correct asymptotic behavior. Phys Rev A 38:3098
24. Becke AD (1993) Density-functional thermochemistry. III. The role of exact exchange. J Chem Phys 98:5648
25. Becke AD (1996) Density-functional thermochemistry. IV. A new dynamical correlation functional and implications for exact-exchange mixing. J Chem Phys 104:1040
26. Lee C, Yang W, Parr RG (1988) Development of the Colle-Salvetti correlation-energy formula into a functional of the electron density. Phys Rev B 37:785

27. Krishna R, Frisch MJ, Pople JA (1980) Contribution of triple substitutions to the electron correlation energy in fourth order perturbation theory. J Chem Phys 72:4244
28. Torkpoor I, Janjanpour MHN, Salehi N, Gharibzadeh F, Edjlali E, (2018) Insight into Y@X2B8 (Y= Li, CO2 and Li-CO2, X = Be, B and C) nanostructures: A computational study. Chem Rev Lett, 1:2-8
29. Sarvestani MRJ, Majedi S (2020) A DFT study on the interaction of alprazolam with fullerene (C20) J Chem Lett, 1:32-38
30. Gharibzadeh F, Gohari S, Nejati K, B. Hashemzadeh B, Mohammadiyan S (2018) The Be atom doping: An effective way to improve the Li-atom adsorptionin boron rich nanoflake of B24. Chem Rev Lett 1:16-22
31. Zhao Y, Truhlar DG (2008) The M06 suite of density functionals for main group thermochemistry, thermochemical kinetics, noncovalent interactions, excited states, and transition elements: two new functionals and systematic testing of four M06-class functionals and 12 other functionals. Theor Chem Accounts 120:215
32. Rostamoghli R, Vakili M, Banaei A, Pourbashir E, Jalalierad K (2018) Applying the B12N12 nanoparticle as a sensor for CO, CO2, H2O and NH3 gasses. Chem Rev Lett 1:31-36
33. Majedi S, Behmagham F, Vakili M (2020) Theoretical view on interaction between boron nitride nanostructures and some drugs. J Chem Lett, 1:19-24
34. Janjanpour MHN, VakiliM, Daneshmehr S, Jalalierad K, Alipour F (2018) Study of the ionization potential, electron affinity and HOMO-LUMO gaps in the small fullerene nanostructures. Chem Rev Lett 1:45-49
35. Moladoust R. (2019) Sensing performance of boron nitride nanosheets to a toxic gas cyanogen chloride: Computational exploring. Chem Rev Lett 2:151-156
36. Koohi M, Bastami H (2020) Structure, stability, MEP, NICS, reactivity, and NBO of Si–Ge nanocages evolved from C_{20} fullerene at DFT. Monatsh Chem 151:693
37. Koohi M, Bastami H (2020) Substituent effects on stability, MEP, NBO analysis, and reactivity of 2,2,9,9-tetrahalosilacyclonona-3,5,7-trienylidenes, at density functional theory. Monatsh Chem 151:11
38. Koohi M, Bastami H (2020) A density functional theory perspective on 2,2,9,9-tetrahalostannacyclonona-3,5,7-trienylidenes. J Phys Org Chem 33:e4031
39. Koohi M, Bastami H (2020) A quest for stable 2,2,9,9-tetrahaloplumbacyclonona-3,5,7-trienylidenes at density functional theory. Struct Chem 31:877
40. Koohi M (2020) Estimating the stability and reactivity of cyclic tetrahalo substituted germylenes: a density functional theory investigation. J Phys Org Chem 33:e4032
41. Vessally E, Nikoorazm M, Esmaili F, Fereyduni E (2011) Substitution effects at α-position of divalent five-membered ring XC_4H_3M (M = C, Si and Ge). J Organomet Chem 696:932
42. Vessally E, Edjlali L, Shabrendi H, Rezaei M (2012) Electronic states of XC_3H_3Si five-membered rings (X = CH, N, P, and As). Russ J Phys Chem 86:595
43. Kassaee MZ, Koohi M (2013) Breathing viability into cyclonona-3,5,7-trienylidenes *via* α-dimethyl and ά-moieties at DFT. J Phys Org Chem 26:540
44. Kassaee MZ, Koohi M, Mohammadi R, Ghavami M (2013) 2,2,9,9-Tetramethylcyclonona-3,5,7-trienylidene *vs.* its heterocyclic analogues: a quest for stable carbenes at DFT. J Phys Org Chem 26:908
45. Koohi M, Kassaee MZ, Haerizade BN, Ghavami M, Ashenagar S (2015) Substituent effects on cyclonona-3,5,7-trienylidenes: a quest for stable carbenes at density functional theory level. J Phys Org Chem 28:514
46. Koohi M (2019) Cyclonona-3,5,7-trienylidene and its Si, Ge, Sn, and Pb analogs versus their α-halogenated derivatives at B3LYP and MP2 methods. J Phys Org Chem 32:e4013
47. Schmidt MW, Baldridge KK, Boatz JA, Elbert ST, Gordon MS, Jensen JH, Koseki S, Matsunaga N, Nguyen KA, Su SJ, Windus TL, Dupuis M, Montgomery JA (1993) General atomic and molecular electronic structure system. J Comput Chem 14(11):1347
48. Sobolewski AL, Domcke W (2002) *Ab initio* investigation of the structure and spectroscopy of hydronium−water clusters. J Phys Chem A 106:4158
49. Hariharan PC, Pople JA (1974) Accuracy of AH, equilibrium geometries by single determinant molecular orbital theory. J Mod Phys 27:209
50. Francl MM, Pietro WJ, Hehre WJ, Binkley JS, Gordon MS, DeFrees DJ, Pople JA (1982) Self-Consistent Molecular Orbital Methods. XXIII. A polarization-type basis set for second row elements. J Chem Phys 77:3654
51. Frisch MJ, Pople JA, Binkley JS (1984) Self-consistent molecular orbital methods 25: supplementary functions for Gaussian basis sets. J Chem Phys 80:3265
52. Clark T, Chandrasekhar J, Spitznagel GW, Schleyer PR (1983) Efficient diffuse function-augmented basis sets for anion calculations. III. The 3-21+G set for first-row elements, Li-F. J Comput Chem 4:294
53. Kendall RA, Dunning Jr TH, Harrison RJ (1992) Electron affinities of the first-row atoms revisited. Systematic basis sets and wave functions. J Chem Phys 96:6796
54. Hehre WJ, Radom L, Schleyer PR, Pople JA (1986) *Ab initio* molecular orbital theory. Wiley, New York
55. Weinhold F, Glendening ED, NBO 7.0 Program manual natural bond orbital analysis programs
56. Weinhold F (2012) Natural bond orbital analysis: a critical overview of relationships to alternative bonding perspectives. J Comput Chem 33:2363
57. Glendening ED, Landis CR, Weinhold F (2012) Natural bond orbital methods. Wiley Interdiscip Rev Comput Mol Sci 2:1
58. Zhang G, Musgrave CB (2007) Comparison of DFT methods for molecular orbital eigenvalue calculations. J Phys Chem A 111:1554
59. Schleyer PVR, Maerker C, Dransfeld A, Jiao H, van Eikema Hommes NJR (1996) Nucleus-independent chemical shifts (NICS): a simple and efficient aromaticity probe. J Am Chem Soc 118:6317
60. Schleyer PR, Jiao H, van Eikema Hommes NJR, Malkin VG, Malkina OL (1997) An evolution of the aromaticity of inorganic rings: refined evidence from magnetic properties. J Am Chem Soc 119:12669
61. Schleyer PVR, Manoharan M, Wang Z, Kiran B, Jiao H, Puchta R, van Eikema Hommes NJR (2001) Dissected nucleus-independent chemical shift analysis of p-aromaticity and antiaromaticity. Org Lett 3(16):2465
62. Domingo LR, Chamorro E, Pérez P (2008) Understanding the reactivity of captodative ethylenes in polar cycloaddition reactions. A theoretical study. J Org Chem 73:4615
63. Parr RG, Szentpaly L, Liu S (1999) Electrophilicity index. J Am Chem Soc 121:1922
64. Parr RG, Pearson RG (1983) Absolute hardness: companion parameter to absolute electronegativity. J Am Chem Soc 105:7512
65. Parr RG, Yang W (1989) Density functional theory of atoms and molecules. Oxford University Press, New York
66. Hoffmann R, Schleyer PR, Schaefer HF (2008) Predicting moleculesdmore realism, Please! Angew Chem Int Ed Eng 47: 7164

67. Joule JA, Mills K (2010) Heterocyclic Chemistry5th edn. Blackwell Publishing, Chichester
68. Alam MJ, Ahmad S (2014) Molecular structure, anharmonic vibrational analysis and electronic spectra of o-, m-, p-iodonitrobenzene using DFT calculations. J Mol Struct 1059:239
69. Koohi M, Bastami H (2020) Substituted Hammick carbenes: the effects of fused rings and hetero atoms through DFT calculations. J Phys Org Chem 33:e4023
70. Boehme C, Frenking G (1996) Electronic structure of stable carbenes, silylenes, and germylenes. J Am Chem Soc 118:2039
71. Jursic BS (1999) Hybrid density functional theory study of low reactivity of imidazol-2-ylidine toward insertion and addition reactions. J Chem Soc, Perkin Trans 2 8:1805